sciendo
Austrian Journal of Earth Sciences | Vienna | 2022 | Volume 115 | 191 - 198 | DOI: 10.17738/ajes.2022.0009

The detachment mechanism of the rockslide causing the Chamoli February 7th, 2021 debris flow disaster

R. Poisel[1], B. Grasemann[2*]
[1)] Vienna University of Technology, Institute of Geotechnics, Karlsplatz 13, 1040 Vienna, Austria
[2)] University of Vienna, Department of Geology, Josef-Holaubek-Platz 2, 1090 Vienna, Austria
[*)] Corresponding author, Bernhard.Grasemann@univie.ac.at

KEYWORDS
Chamoli disaster 2021, mechanics of rock failure, back analysis, natural hazard

Abstract

On February 7th, 2021, a rockslide of about 20 Mio m^3 detached in a height of 5600 m asl. from the northern flank of Mount Ronti (Chamoli district, Uttarakhand state, India), turned into a rock mass fall and produced a debris flow. When the rock mass hit the Ronti Gad valley after a fall height of 1800 m the rock mass mixed with melting dead ice together with snow and ice avalanche material of previous debris flows. The debris flow destroyed hydroelectric infrastructure between 10 - 20 km down the valley killing 204 people either working at or visiting the power plants. By combining remote sensing, structural geology and kinematics/mechanical analysis of the rockslide, we demonstrate that a 600 m wide and almost 800 m long block of quartzite, bordered laterally by two joints and a newly formed tension crack on the top detached from an underlying layer of biotite-rich paragneisses. Assuming full hydrostatic heads in both joints and in the tension crack as well as 75% of the full hydrostatic head in the lower boundary surface between quartzites and paragneisses, the rock block analysis yields a friction angle of 32° for both joints, which is a plausible value of the friction angle of joints in quartzites. The detachment of the block has been the result of the widening of the tension crack on top, of a progressive propagation of the lateral joints together with a catastrophic failure of the detachment plane at the border between quartzites and paragneisses. At the time of the failure, all discontinuities must have been almost completely filled with water raising the question, if the frequency of rockslides in the Himalayas is increasing as temperatures rise and permafrost is thawing due to climate change.

1. Introduction

On February 7th, 2021, a rockslide of about 20 Mio m^3 covered with ice and snow with coordinates UTM44 378370E 3360900N detached in a height of about 5600 m asl. from the north flank of Mount Ronti (Chamoli district, Uttarakhand state, India). It turned into a rock mass fall, which is characterized by the detachment of a coherent rock mass fragmenting into individual blocks (Corominas et al., 2017), damming up the Ronti Gad valley 1800 m deeper and melting dead ice, due to high kinetic energy (Petley, 2021a). After the breakthrough of the landslide dam the evolving debris flow entrained large volumes of water from melted dead ice together with snow and ice avalanche material of former events on its way down the Rishi Ganga valley (Fig. 1). A similar case, where a debris flow developed from mixing with large volumes of water occurred 2017 in Graubünden (Switzerland), when a rock mass fall detached from the North-face of Pizzo Cengalo, eroded and melted glacial ice and transformed into a debris flow which reached the town of Bondo (Wilhelm et al., 2019; Walter et al., 2020).

10 km downstream, south of Raini village at the confluence of the Rishi Ganga and Dhauli Ganga rivers, the 13.2 MW Rishi Ganga hydropower project was completely destroyed. Another 10 km downstream the Tapovan-Vishnugad hydropower project was severely damaged. Another 15 km downstream, a river gauge at Joshimath, a city of more than 17000 people where the Dhauli Ganga meets the Alaknanda River, measured its highest water level ever recorded in history. During the disaster 204 people, most of which were workers and visitors in a gallery of Tapovan-Vishnugad hydropower project lost their lives out of which only 72 bodies have been recovered (PTI, 2021).

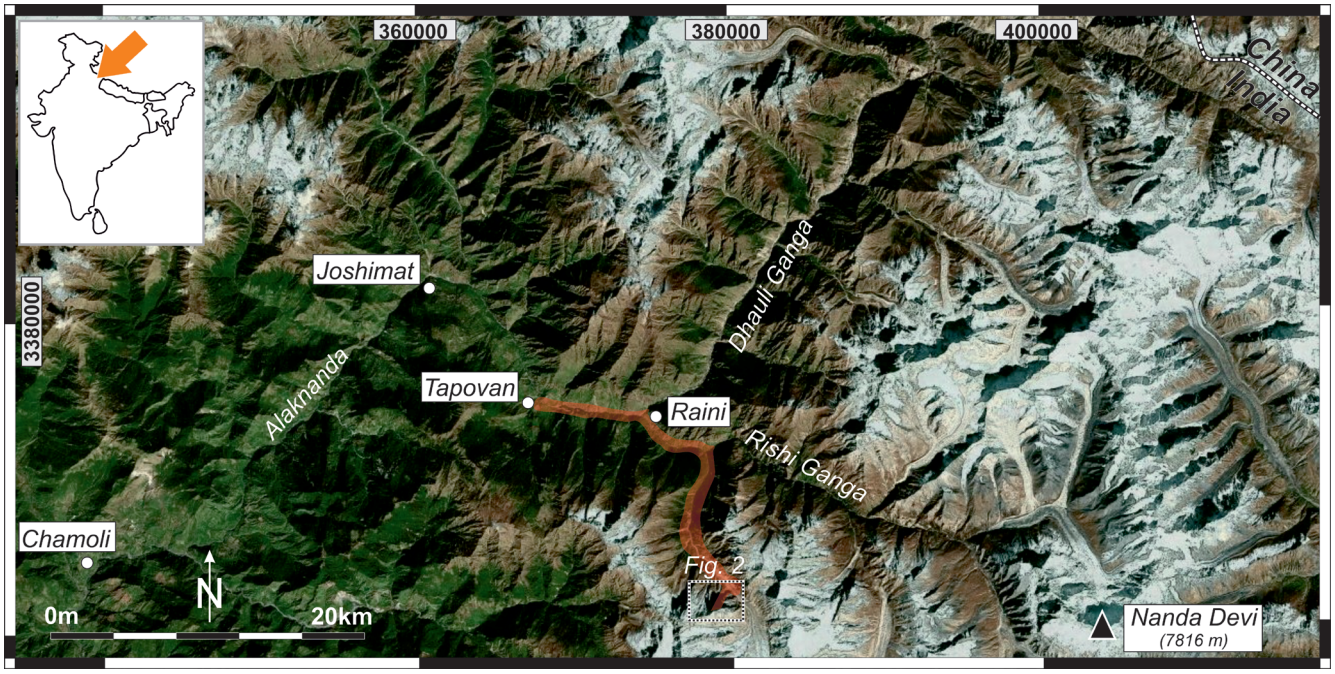

Figure 1: Satellite image (Microsoft, 2022) of NE Uttarakhand (N India) showing the location of the investigated rockslide in Figure 2 (white dotted rectangle). The image shows the area before failure. Coordinates are given in UTM 44. Red transparent area gives the extent of dust and debris associated with the slide on February 7th, 2021.

While the potential processes, which led to the giant debris flow, are discussed in Shugar et al. (2021) and on various blogs and social media (e.g. Petley, 2021a and b), the focus of this short study is the mechanics of the rockslide detachment. Immediately after the disaster the debris flow has been attributed to a glacial lake outburst or to an ice avalanche. However, already on February 11th, 2021, Petley (2021b) presented on his blog a Planet Labs SkySat image showing the niche created by a rock block failure. Berthier and Gascoin (2021) presented profiles showing elevation changes in the source area determined by a comparison of a 4 m resolution Pléiades Digital Elevation Model (DEM) from February 10th, 2021, and a Copernicus 30 m resolution DEM from 2013. By combining these observations, with remotes sensing, structural geology and rock mechanics, this study contributes to the geometry and the mechanics of the rock failure causing the Chamoli debris flow disaster.

2. Methods

2.1 Remote sensing and Geographic Information System (GIS)

The area around the landslide was investigated by remote sensing techniques based on satellite images from bing maps (Microsoft, 2022) and digital elevation data from the Shuttle Radar Topography Mission (SRTM, USGS, 2022a) combined in a QGIS project (QGIS, 2022a). The satellite image was imported into QGIS using the standard OpenLayers Plugin Tool. Shuttle Radar Topography Mission data were imported using the SRTM-Downloader plugin (QGIS, 2022b). The void filled data have a resolution of 1 arc-second (30 meters). Elevation contour lines with an interval spacing of 250 m were extracted from the SRTM data using the standard QGIS Raster-Extraction tool. Spatial orientation data of the foliation and joint pattern were calculated using the 3-point methods from the QGIS project by extracting x-y-z data from three points on a planar structure (x: UTM 44 east, y: UTM 44 north and z: elevations from the SRTM). Since the measured structures can be traced over several hundreds of meters the error introduced by the 30 m resolution elevation data is less than 5°.

2.2 Geomechanical analysis

The aim of the analysis was to back calculate the friction angle of the joints in the quartzites, using the theory of limit equilibrium assuming a rigid block. It was also assumed that all forces pass through its centre of gravity and therefore no rotations occur (as known from other sliding wedge cases, e.g. Wylie, 2017). The method is based on the question whether the resulting friction angle corresponds with values known from the literature and if so, which conditions (e.g., water pressures on the boundary planes of the rock block) are necessary to result in this friction angle. Petley (2021a) suggested that the detachment mechanism had been a wedge failure. A kinematic check (see below) of the geometric conditions of the block proved this mechanism to be possible. As a first order estimation the friction angle of the sliding planes (joints in the quartzites) was back calculated for the case without water pressures on the boundary planes of the rock block using the formulae given by

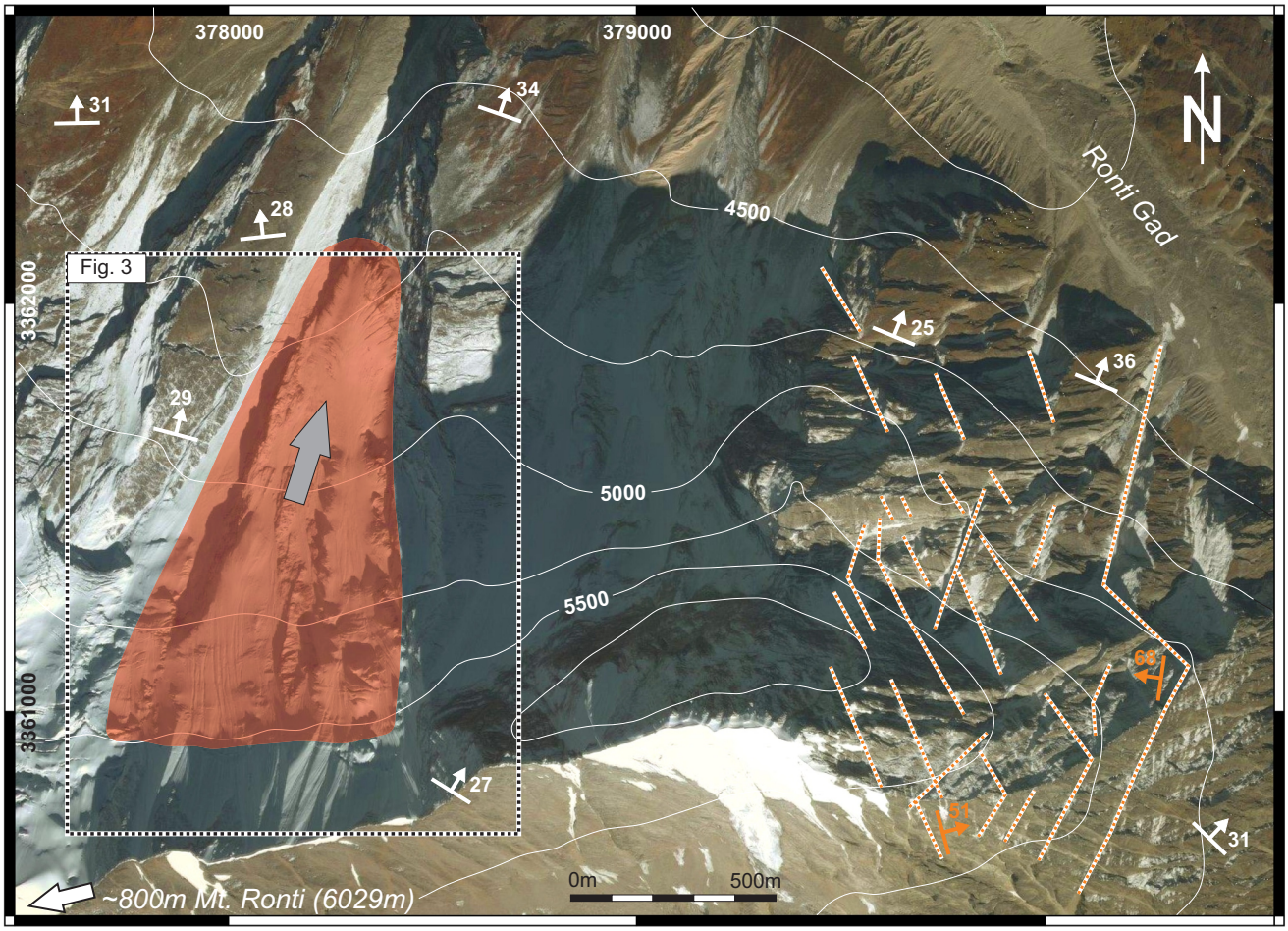

Figure 2: Satellite image (Microsoft, 2022) of the location of the rock failure (red transparent wedge) in the N face of Mount Ronti. Grey arrow gives the sliding direction of the failed block. The image shows the area after failure. White tectonic symbols show the dip-direction and dip angle of the main foliation in the rocks calculated with the 3-point-method from the SRTM digital elevation model. Orange dotted lines show the traces of conjugate sets of steeply W- and E- dipping joint systems. Orange tectonic symbols show the dip-direction and dip angles representative for these joints. White contour lines represent elevations in meter with a contour interval of 250 m. Black dotted rectangle shows the exact location of Figure 3.

Hoek and Bray (1981) and by Wyllie (2017) considering only the weight of the block. As the friction angle turned out to be too low, a vector analysis at limit equilibrium was performed considering also water pressures on the boundary planes of the rock block. The analysis did not follow the procedure given by Hoek and Bray (1981) and by Wyllie (2017) because the aim was not a determination of a factor of safety, but a back calculation of the angle of friction of the joints using a simplified geometry of the investigated rockslide. This analysis yielded a realistic angle of friction of the joints in quartzites when the joints and the tension crack have been filled completely with water and the base plane by 75% to reach limit equilibrium and failure. For the sake of clarity, the used equations and the individual steps are introduced in the worked example of the rock block analysis.

3. Geological setting

The investigated area is located in the Garhwal Himalayas in northern India west of the Nanda Devi National Park hosting the highest peak (Nanda Devi, 7816 m) entirely located in Uttarakhand (India). The Alaknanda, Dhauli Ganga and Rishi Ganga river drain the Garwahl Himalayas. Tectonic uplift and the intense fluvial incision result in long steep slopes that are prone to failure (Barnard et al., 2021).

Geologically, the investigated rock mass fall is located in the so called Munsiari Formation, which is a 500-700 m thick mylonitic shear zone below the high-grade metamorphic Proterozoic–Cambrian Higher Himalayan Crystalline rocks and above the low-grade Proterozoic rocks of the Lesser Himalayan Sequence (Hodges, 2000). Lithologically, the Munsiari Formation consists of bright mylonitic muscovite-quartz schists and quartzites interlayered with layers of dark biotite-rich paragneisses (Jain et al., 2014; Hunter et al., 2018). Whereas the more competent quartz-rich lithologies form meter-thick packages, the less competent interbedded layers of paragneisses are strongly sheared phyllonites, recording top-to-the south shear sense (Jain et al., 2014; Hunter et al., 2018).

Using the 3-point methods at several locations in the investigated area (see tectonic symbols in Fig. 2)

		dip direction	dip
intersection line of joints 1 and 2	$\mathbf{i_{12}}$	015	22
trace of joint 1	$\mathbf{t_1}$	083	46
trace of joint 2	$\mathbf{t_2}$	263	60
strike vector of the plane normal to the line of intersection	**s**	285	00
dip vector of the plane normal to the line of intersection	**d**	195	68
vertical	**v**	000	90
vector normal to tension crack	$\mathbf{t_c}$	352,5	00
vector normal to base plane (pointing upwards)	**b**	352,5	54

Table 1: Dip directions and dip angles of geometrical vectors used in the rock block analysis.

the strongly foliated rocks of the mylonitic Munsiari Formation weather in planar surfaces, which dip with about 25-35° towards N to NE and have a pronounced stretching lineation trending NNE-SSW, which can be even identified in the satellite images. The sequence is intensely fractured by a conjugate set of brittle, roughly W and E dipping joints. Typical values for the joint sets derived from the 3-point method are 075/50 and 280/70 (Fig. 2). Most joints have a strike length of less than a few 100 meters although some joints can be traced in the satellite images over a strike length of more than 3 kilometres (Fig. 2). The confined length of the joints in the satellite image may suggests that the joints are probably decoupled at lithological boundaries, most likely between the more competent quartzites and the less competent biotite-rich paragneisses. Since no offsets of markers are observed in the satellite images, the joints have not been significantly reactivated as faults and most likely contain incohesive cataclasites or fault gauges only to a minor degree. The thick mylonitic packages with planar foliation surfaces and visible stretching lineation are most likely high-grade quartzites reported from outcrops along the strike of the lithologies in the Alaknanda valley (Jain et al., 2014). These quartzites show a gradual transition into dark layers in the S-face of Mount Ronti and may correlate to the biotite-rich paragneisses (Hunter et al., 2018).

The whole state of Uttarakhand is known for the active tectonics and the high seismicity with more than 50 historically known earthquakes between M_w 5 and 7 (USGS, 2022b). However, for the following discussion it is important to note that the only earthquake, which occurred in the first week of February 2021, was on 2nd February 2021 about 500 km to the ESE with the Moment Magnitude of M_w 4.5 and therefore an earthquake triggered rockslide can be excluded (compare the shake map at earthquake.usgs.gov).

4. Rock block analysis

Figure 3 shows a Planet Labs SkySat image (Planet Team, 2021) of the source after the rockslide causing the Chamoli debris flow disaster. As mentioned above, Petley (2021a) suggested that the detachment mechanism had been a wedge failure. Figure 3 displays the two joints forming the block, the boundary surface between quartzites (bright) and paragneisses (dark) which is the detachment or base plane of the block, the newly formed tension crack bordering the rock block to the south, and the positions of the profiles given by Berthier and Gascoin (2021). Profiles a and b (Fig. 4) give the orientations of the intersection line of joints 1 and 2 as well as of the traces of joints 1 and 2 in profile b (Table 1) in a right-hand coordinate system +x = E, +y = N, +z pointing upwards. As shown by the orthoimage given by Berthier and Gascoin (2021) the dip direction of the slope surface is to the north and the dip angle is 42° slightly steeper than the regional main metamorphic foliation of the rocks derived by the 3-point method. Thus, the apparent dip of the slope surface in profile a (Figure 4) is 41°. The base plane strikes S 82 W - N 82 E, therefore the dip direction is 352°. The (true) dip follows from the apparent dip of 34° (Fig. 4) with 36°.

As described in the geological setting chapter above, the joints developed predominantly in the more competent quartzites and are not observed in the satellite image in the dark paragneiss layers. Therefore, the rock block has the shape of a truncated wedge as shown in profile b in Figure 4 and in Figure 5. Table 1 lists the orientations of vectors necessary for the rock block analysis. The cross products $\mathbf{i}_{12} \times \mathbf{t}_1$ and $\mathbf{t}_2 \times \mathbf{i}_{12}$ give the vectors normal to joints 1 and 2 (Tab. 2; vectors are in bold). The spatial orientation given in dip direction and dip angle of joint 1 is 081/46, the orientation of joint 2 is 297/64. Figure 6 shows that the intersection vector of joint 1 and joint 2, which is the movement direction of the block, points from the slope face into the free space meaning that the block could detach from the slope surface. Figure 6 also reveals that the block has been sliding on both joints surfaces and not on one joint only (Goodman and Shi, 1985). The acute angle between the direction of movement of the block and the base plane has caused a tensile as well as a shear loading of the detachment plane between quartzites and paragneisses. This hybrid loading of the detachment plane caused a lift-off of the

		x	y	z	Length of vector
vector normal to joint 1	$\mathbf{n_1}$	- 0.604	- 0.098	- 0.591	0.851
vector normal to joint 2	$\mathbf{n_2}$	0.796	-0.400	- 0.425	0.987

Table 2: Vectors normal to joint 1 and joint 2 bordering the investigated block.

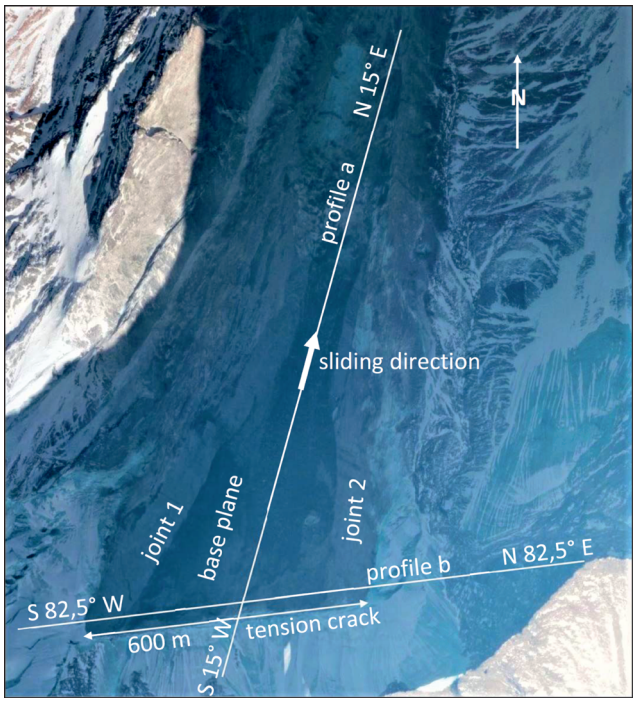

Figure 3: Planet Labs SkySat image of the source after the rockslide (used with permission from Planet Team, 2021). Note the dark colour of the base plane (paragneiss) below the bright colours of the quartzite. For location and coordinates compare Figure 2.

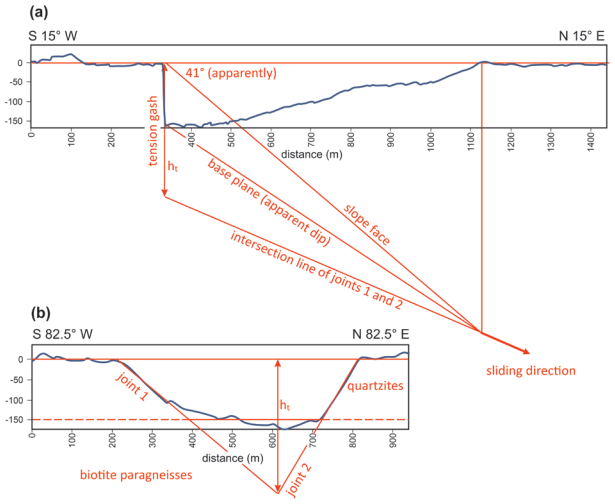

Figure 4: Undistorted elevation changes in profiles (for location see Figure 3) after Berthier and Gascoin (2021). Blue: measured elevation changes; red: approximated geometry of wedge; h_t: depth of intersection line of joints 1 and 2 in the tension crack a) Profile a in the dip direction of the intersection line of joints 1 and 2 (= sliding direction; NNE-SSW). b) Profile b parallel to the strike of the tension gash (WSW-ENE).

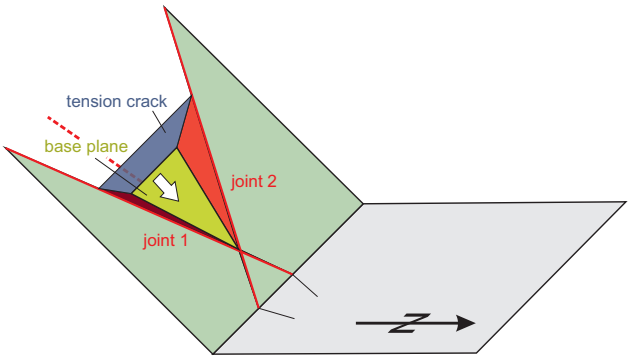

Figure 5: Oblique view of simplified geometry of the detachment niche used for calculations in the rock block analysis. The base plan of the wedge is the detachment surface between the quartzites and the paragneisses shown as a yellow surface. The green surface indicates the surface slope. The blue surface represents the tension crack. The red dashed line indicates the intersection lineation of joint 1 and joint 2. The white arrow indicates the direction of sliding.

quartzite wedge and therefore the detachment plane must have been propagated across the whole base plane of the wedge before the block slid downwards.

As a first order estimation of the friction angle of joints 1 and 2 we applied a back analysis considering only the weight of the block. A friction only analysis was chosen because of the strike length of the joints observed in the satellite image. As mentioned above, the rock block has been sliding on both joints. Therefore, at limit equilibrium, the sum of the reactions normal to the joints times the tangent of the friction angle, must have been equal to the block weight times the sine of the intersection dip (Hoek and Bray, 1981; Wyllie, 2017). Resolving the contact forces horizontally and vertically in a plane normal to the line of intersection, the condition for limit equilibrium gives:

$$\frac{W\cos\alpha_i \sin\beta}{\sin\frac{\xi}{2}}\tan\varphi = W\sin\alpha_i \tag{1}$$

$$\frac{\tan\varphi \sin\beta}{\sin\frac{\xi}{2}} = \tan\alpha_i \tag{2}$$

$$\varphi = \tan^{-1}\frac{\sin\frac{\xi}{2}\tan\alpha_i}{\sin\beta} \tag{3}$$

where W is the weight of the rock block, ϕ angle of friction along joints 1 and 2, ξ is the angle between the joints α_i is the dip angle of the line of intersections between the

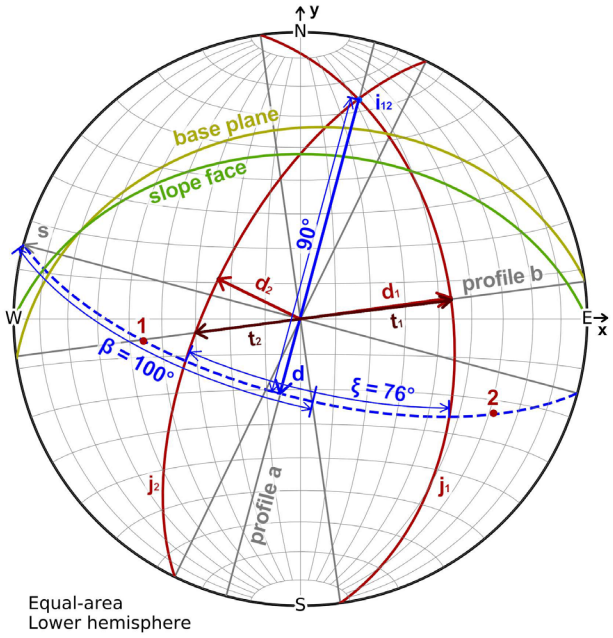

Figure 6: Equal area stereoplot (lower hemisphere) of discontinuities bordering the detached quartzite wedge. For abbreviations of geometrical vectors see Table 1.

joints and β is the angle between the strike of the plane normal to the line of intersection and the normal to joint 2 (i.e. the pole of joint 2) minus 90° plus $\xi/2$ (Fig. 6).

Using the dot product $\mathbf{n}_1 \cdot \mathbf{n}_2$ yields ξ = 76.4°. The dot product $\mathbf{s} \cdot \mathbf{n}_2$ yields 152.2° and hence β = 152.2° – 90° + 38.2° = 100.4°. Using the condition for limit equilibrium, the angle of friction ϕ is 14°. Considering that most likely the joints contain incohesive cataclasites or fault gauges only to a minor degree, this value seems to be much too low. Typically, friction angles of joints in quartzites are between 30° and 35° (Wyllie, 2017).

5. Discussion

As described above, an earthquake can be eliminated as the trigger of the rockslide. By analogy with the Pizzo Cengalo 2017 3.0 x 10^6 m^3 rockslide in Switzerland, which was favoured by permafrost conditions and caused the catastrophic Bondo debris flow (Walter et al., 2020), only images of the detachment niche have been available to decide whether hydraulic and/or ice thrust contributed to the detachment (Wilhelm et al., 2019). The image of the Chamoli rockslide detachment niche (Fig. 3) as well as the image used by Berthier and Gascoin (2021) and Shugar et al. (2021) do neither show any ice in the joints nor on the detachment plane and therefore we assume that only hydraulic thrust contributed to the detachment.

As discussed above, the detachment or base plane is the result of a hybrid tensile and shear loading of the border between the quartzites and the paragneisses. After a basal fracture propagated along the detachment plane, sliding of the quartzite block along the line of intersection has been possible accompanied by lift-off of the quartzite block from the paragneisses. Therefore, we assume that the detachment plane has been moistened only to a limited extent when limit equilibrium has been reached and failure occurred. The hydrostatic force acting on the base plane is therefore considered only by 75%.

Considering hydrostatic forces in joints 1 and 2, in the tension crack as well as in the base plane, the limit equilibrium condition is constrained by:

$$(R_1 + R_2)\tan\varphi = \sum F_i \qquad (4)$$

where $R_{1,2}$ are normal reactions in joints 1 and 2, ΣF_i the sum of the components of W, H_{j1}, H_{j2}, H_t, H_b parallel to the intersection line of joints 1 and 2. $H_{j1,2}$ are the hydrostatic forces in joints 1 and 2, H_t is the hydrostatic force in the tension crack and H_b is the hydrostatic force in the base plane. The components of W, H_{j1}, H_{j2}, H_t, H_b parallel to the intersection line of joints 1 and 2 can be found by applying the dot products (lengths of $\mathbf{i}_{12}$, $\mathbf{v}$, $\mathbf{n}_1$, $\mathbf{n}_2$, $\mathbf{t}_c$, $\mathbf{b}$ = 1): $\mathbf{i}_{12} \cdot \mathbf{v}\, W$, $\mathbf{i}_{12} \cdot \mathbf{n}_1\, H_{j1}$, $\mathbf{i}_{12} \cdot \mathbf{n}_2\, H_{j2}$, $\mathbf{i}_{12} \cdot \mathbf{t}_c\, H_t$, $\mathbf{i}_{12} \cdot \mathbf{b}\, H_b$. Inserting W = 468.896 MN, H_{j1} = 38.594 MN, H_{j2} = 36.050 MN, H_b = 127.313 MN (i.e. 75% of 169.750) and H_t = 48.375 MN (values determined using stereometric formulae) the sum of components parallel to the intersection line of joints 1 and 2 ΣF_i = 242,608 MN. R_1 and R_2 can be determined resolving equilibrium in the strike and dip directions of the plane normal to the intersection line:

$$R_1 \sin\left(\beta - \frac{\xi}{2}\right) - R_2 \sin\left(\beta + \frac{\xi}{2}\right) - \sum F_s = 0 \qquad (5)$$

$$R_1 \cos\left(\beta - \frac{\xi}{2}\right) - R_2 \cos\left(\beta + \frac{\xi}{2}\right) - \sum F_d = 0 \qquad (6)$$

where ΣF_s is the sum of the components of W, H_{j1}, H_{j2}, H_t, H_b parallel to the strike of the plane normal to the intersection line of joints 1 and 2 and ΣF_d is the sum of the components of W, H_{j1}, H_{j2}, H_t, H_b parallel to the dip vector of the plane normal to the intersection line of joints 1 and 2. Following the procedure used to calculate ΣF_i, ΣF_s = - 53,464 MN and ΣF_d = 250,863 MN. Solving Equations 5 and 6 yields R_1 = 129,761 MN, R_2 = 253,955 MN and $R_1 + R_2$ = 383,716 MN. Using Equation 4 results in an angle of friction ϕ = 32°. Therefore, the joints and the tension crack must have been filled completely with water and the base plane by 75% to reach limit equilibrium and failure.

6. Conclusions

Based on remote sensing and structural geology of the investigated area, the analyses of the geometry and the mechanics of the Chamoli February 7th, 2021 rockslide have shown that a rock block cut out of a quarzitic layer by two joints and a newly formed tension crack slid down on these two joints. The lower boundary surface of the block has resulted from a hybrid tensile and shear loading of the border between quartzites and paragneisses caused by an acute angle between the intersection line

of the two joints and the lower boundary surface. Its irregularities shown in Figure 4 reveal that the fracture has not followed a predetermined discontinuity. It has developed progressively from a propagating fracture forming a detachment plane, before the block has slid downwards and has lifted off the paragneisses.

The mechanical analysis of the block detachment considering only the weight of the block yields a friction angle of the joints of 14° in order to meet limit equilibrium. Considering that the joints were not lubricated by either incohesive cataclasites or clay gauges, this value by far too low. Therefore, we conclude that hydraulic and/or ice thrust contributed to the detachment of the quartzite block. Considering full hydrostatic heads in both joints and in the tension crack and 75% of the full hydrostatic head along the detachment surface between quartzites and paragneisses, the back analysis yields a friction angle of both joints of 32°, which is a plausible value of the friction angle of a joint in quartzites.

We conclude that the detachment of the block has been the final result of a progressive formation of the tension crack, of propagation of the joints as well as the progressive formation of the fracture at the border between quartzites and paragneisses forming the detachment surface associated with infiltration of water into all discontinuities over an extended period (van Wyk de Vries et al., 2021). This conclusion contributes to the discussion about the frequency of rockslides in high-alpine regions, which may increase in future due to temperature rise and shift of the lower permafrost limits (e.g. Schrott et al., 2012; Duvillard et al., 2021; Arenson et al., 2022).

Acknowledgements

Part of the work was funded by the Austrian Science Foundation FWF (project POLARIS, grant number I5399-N). We thank the Associate Editor Hugo Ortner for efficient handling of our manuscript, and Florian Amann and an anonymous reviewer for thorough reviews, which significantly improved our manuscript in both content and style.

References

Arenson, L.U., Harrington, J.S., Koenig, C.E.M., Wainstein, P.A., 2022. Mountain Permafrost Hydrology—A Practical Review Following Studies from the Andes. Geosciences, 12, 48. https://doi.org/10.3390/geosciences12020048.

Barnard, P.L., Owen, L.A., Sharma, M.C., Finkel, R.C., 2001. Natural and human-induced landsliding in the Garhwal Himalaya of northern India. Geomorphology, 40/1–2, p. 21–35. https://doi.org/10.1016/S0169-555X(01)00035-6.

Berthier, E., Gascoin, S., 2021. Pléiades images of the Uttarakhand disaster. Centre d'Etudes Spatiales de la Biosphère https://labo.obs-mip.fr/multitemp/pleiades-images-of-the-uttarakhand-disaster/ (accessed on 18 November 2022).

Corominas, J., Mavrouli, O., Ruiz-Carulla, R., 2017. Rockfall Occurrence and Fragmentation. In: Sassa, K., Mikos, M., Yin, Y. (eds.), Advancing Culture of Living with Landslides Springer International Publishing AG, Cham, p. 75–97. https://doi.org/10.1007/978-3-319-59469-9_4.

Duvillard, P.-A., Ravanel, L., Schoeneich, P., Deline, P., Marcer, M., 2021. Qualitative risk assessment and strategies for infrastructure on permafrost in the French Alps. Cold Regions Science and Technology, 189, 103311 https://doi.org/10.1016/j.coldregions.2021.103311.

Goodman R.E., Shi, G.-h., 1985. Block Theory and its application to rock engineering. Prentice-Hall, Englewood Cliffs, 338 pp.

Hodges, K.V., 2000. Tectonics of the Himalaya and southern Tibet from two perspectives. Geological Society of America Bulletin, 112/3, p. 324–350. https://doi.org/10.1130/00167606(2000)112<324:TOTHAS>2.0.CO;2.

Hoek, E., Bray, J.W., 1981. Rock slope engineering. The Institution of Mining and Metallurgy, London, 368 pp.

Hunter, N.J.R., Weinberg, R.F., Wilson, C.J.L., Luzin, V., Misra, S., 2018. Microscopic anatomy of a "hot-on-cold" shear zone: Insights from quartzites of the Main Central Thrust in the Alaknanda region (Garhwal Himalaya). Geological Society of America Bulletin, 130/9–10, p. 1519–1539. https://doi.org/10.1130/B31797.1.

Jain, A.K., Shreshtha, M., Seth, P., Kanyal, L., Carosi, R., Montomoli, C., Iaccarino, S., Mukherjee, P.K., 2014. The Higher Himalayan Crystallines, Alaknanda – Dhauli Ganga Valleys, Garhwal Himalaya, India. Journal of the Virtual Explorer, 47/8, p. 1–34. https://doi.org/10.3809/jvirtex.2014.00349.

Microsoft, 2022. Bing Maps, Microsoft Bing. https://www.bing.com/maps/ (accessed on 18 November 2022).

Petley, D., 2021a. The catastrophic landslide and flood in Chamoli in Uttarakhand: the sequence of events. The Landslide Blog, American Geophysical Union, Washington DC. https://blogs.agu.org/landslideblog/2021/02/08/chamoli-2/ (accessed on 18 November 2022).

Petley, D., 2021b. High resolution Planet Labs imagery of the Chamoli landslide in Uttarakhand. The Landslide Blog, American Geophysical Union, Washington DC. https://blogs.agu.org/landslideblog/2021/02/11/chamoli-landslide-3/ (accessed on 18 November 2022).

Planet Team, 2021. Planet Application Program Interface: In Space for Life on Earth. San Francisco, CA. https://www.planet.com (accessed on 18 November 2022).

PTI, 2021. Uttarakhand assembly condoles deaths in Chamoli disaster. The New Indian Express, Chennai. https://www.newindianexpress.com/nation/2021/mar/02/uttarakhand-assembly-condoles-deaths-in-chamoli-disaster-2271196.html (accessed on 18 November 2022).

QGIS, 2022a. QGIS Installers. QGIS Development Team. https://www.qgis.org/en/site/forusers/alldownloads.html (accessed on 5 April 2022).

QGIS, 2022b. SRTM-Downloader 3.1.17. QGIS Python

Plugins Repository. https://plugins.qgis.org/plugins/SRTM-Downloader/version/3.1.17/ (accessed on 5 April 2022).

Schrott, L., Otto, J.-C., Keller, F., 2012. Modelling alpine permafrost distribution in the Hohe Tauern region, Austria. Austrian Journal of Earth Sciences, 105/2, p. 169–183.

Shugar, D. H., Jacquemart, M., Shean, D., Bhushan, S., Upadhyay, K., Sattar, A., Schwanghart, W., McBride, S., Vries, M. V. W. d., Mergili, M., Emmer, A., Deschamps-Berger, C., McDonnell, M., Bhambri, R., Allen, S., Berthier, E., Carrivick, J. L., Clague, J. J., Dokukin, M., Dunning, S. A., Frey, H., Gascoin, S., Haritashya, U. K., Huggel, C., Kääb, A., Kargel, J. S., Kavanaugh, J. L., Lacroix, P., Petley, D., Rupper, S., Azam, M. F., Cook, S. J., Dimri, A. P., Eriksson, M., Farinotti, D., Fiddes, J., Gnyawali, K. R., Harrison, S., Jha, M., Koppes, M., Kumar, A., Leinss, S., Majeed, U., Mal, S., Muhuri, A., Noetzli, J., Paul, F., Rashid, I., Sain, K., Steiner, J., Ugalde, F., Watson, C. S., Westoby, M. J., 2021. A massive rock and ice avalanche caused the 2021 disaster at Chamoli, Indian Himalaya. Science, 37/6552, p. 300–306. https://doi.org/10.1126/science.abh4455

USGS, 2022a, EarthExplorer (EE). United States Geological Survey, Reston. https://earthexplorer.usgs.gov/ (accessed on 18 November 2022).

USGS, 2022b. Earthquake hazards program. United States Geological Survey, Reston. https://earthquake.usgs.gov/ (accessed on 18 November 2022).

van Wyk de Vries, M., Bhushan, S., Shean, D., Berthier E, Deschamps-Berger, C., Gascoin, S., Jacquemart, M., Kääb, A., Shugar, D., 2021. Resolving pre-collapse slope motion at the February 2021 Chamoli rock-ice avalanche via feature tracking of optical satellite imagery. EGU General Assembly 2021, EGU21-16597.

Walter, F., Amann, F., Kos, A., Kenner, R., Phillips, M., de Preux, A., Huss, M., Tognacca, C., Clinton, J., Diehl, T., Bonanomi, Y., 2020. Direct observations of a three million cubic meter rock-slope collapse with almost immediate initiation of ensuing debris flows. Geomorphology, 351, 106933. https://doi.org/10.1016/j.geomorph.2019.106933

Wilhelm, C., Feuerstein, G.C., Huwiler, A., Kühne, R., 2019. Bergsturz Cengalo und Murgänge Bondo: Erfahrungen der kantonalen Fachstelle. In: Bründl, M., Schweizer, J. (eds.), Lernen aus Extremereignissen. Eidgenössische Forschungsanstalt für Wald, Schnee und Landschaft WSL Berichte, 78, p. 53–66.

Wyllie, D.C., 2017. Rock slope engineering. 5th edition. CRC Press, Boca Raton, 636 pp. https://doi.org/10.4324/9781315154039

Received: 1.3.2022
Accepted: 6.12.2022
Editorial Handling: Hugo Ortner